Journal of Arrhythmia 31 (2015) 152–158

Contents lists available at ScienceDirect

Journal of Arrhythmia

journal homepage: www.elsevier.com/locate/joa

Original Article

Visualization of the radiofrequency lesion after pulmonary vein isolation using delayed enhancement magnetic resonance imaging fused with magnetic resonance angiography

Kunihiko Kiuchi, MD[a,*], Katsunori Okajima, MD[a], Akira Shimane, MD[a], Kiminobu Yokoi, MD[a], Jin Teranishi, MD[a], Kousuke Aoki, MD[a], Misato Chimura, MD[a], Hideo Tsubata, MD[a], Taishi Miyata, MD[a], Yuuki Matsuoka, MD[a], Takayoshi Toba, MD[a], Shogo Ohishi, MD[a], Takahiro Sawada, MD[a], Yasue Tsukishiro, MD[a], Tetsuari Onishi, MD[a], Seiichi Kobayashi, MD[a], Shinichiro Yamada, MD[a], Yasuyo Taniguchi, MD[a], Yoshinori Yasaka, MD[a], Hiroya Kawai, MD[a], Kazushi Ikeuchi, RT[b], Yutaka Shigenaga, RT[b], Takayuki Ikeda, RT[b]

[a] Department of Cardiology, Himeji Cardiovascular Center, 520 kou saishou, Himeji, Hyogo, Japan
[b] Department of Laboratory and Radiology, Himeji Cardiovascular Center, 520 kou saishou, Himeji, Hyogo, Japan

ARTICLE INFO

Article history:
Received 13 September 2014
Received in revised form
5 October 2014
Accepted 28 October 2014
Available online 27 November 2014

Keywords:
Delayed enhancement MRI
MRA
Radiofrequency lesions
Atrial fibrillation
Catheter ablation

ABSTRACT

Background: The radiofrequency (RF) lesions for atrial fibrillation (AF) ablation can be visualized by delayed enhancement magnetic resonance imaging (DE-MRI). However, the quality of anatomical information provided by DE-MRI is not adequate due to its spatial resolution. In contrast, magnetic resonance angiography (MRA) provides similar information regarding the left atrium (LA) and pulmonary veins (PVs) as computed tomography angiography. We hypothesized that DE-MRI fused with MRA will compensate for the inadequate image quality provided by DE-MRI.
Methods: DE-MRI and MRA were performed in 18 patients who underwent AF ablation (age, 60 ± 9 years; LA diameter, 42 ± 6 mm). Two observers independently assessed the DE-MRI and DE-MRI fused with MRA for visualization of the RF lesion (score 0–2; where 0: not visualized and 2: excellent in all 14 segments of the circular RF lesion).
Results: DE-MRI fused with MRA was successfully performed in all patients. The image quality score was significantly higher in DE-MRI fused with MRA compared to DE-MRI alone (observer 1: 22 (18, 25) vs 28 (28, 28), $p < 0.001$; observer 2: 24 (23, 25) vs 28 (28, 28), $p < 0.001$).
Conclusions: DE-MRI fused with MRA was superior to DE-MRI for visualization of the RF lesion owing to the precise information on LA and PV anatomy provided by DE-MRI.

1. Introduction

Pulmonary vein isolation (PVI) is the cornerstone of ablation for atrial fibrillation (AF) [1,2]. We have previously reported that the radiofrequency (RF) lesion can be visualized with delayed enhancement magnetic resonance imaging (DE-MRI) [3]. However, visualization of the RF lesion gap, especially that located at the anterior ridge or carina, was difficult in some patients for the following reasons: (1) The anatomy of the anterior ridge between the left pulmonary vein (LPV) and left atrial appendage (LAA) and the carina between the superior PV and inferior PV is complex and varied among patients. (2) The spatial resolution of DE-MRI is not adequate for visualization of complex anatomy. Recently, magnetic resonance angiography (MRA) was reported to provide similar information on the left atrium (LA) and PV anatomy as contrast-enhanced computed tomography angiography (CTA) [4]. Thus, we hypothesized that DE-MRI fused with MRA compensates for the inadequate quality of the anatomical information provided by DE-MRI alone.

Abbreviations: RF, radiofrequency; AF, atrial fibrillation; DE-MRI, delayed enhancement magnetic resonance imaging; MRA, magnetic resonance angiography; LA, left atrium; PV, pulmonary vein

* Corresponding author. Tel.: +81 79 293 3131; fax: +81 79 295 8199.
E-mail address: kunihikokiuchi@yahoo.co.jp (K. Kiuchi).

http://dx.doi.org/10.1016/j.joa.2014.10.003
1880-4276/

2. Material and methods

2.1. Patient selection

Eighteen consecutive patients who underwent AF ablation were included in the study. All patients underwent contrast-enhanced MRI using a 1.5-T MR system (Intera Achiva; Philips Medical Systems, Best, the Netherlands) equipped with a 32-channel cardiac coil. In this study, MRI consisted of contrast-enhanced MRA (CE-MRA) and DE-MRI. DE-MRI and MRA scans were interpretable in all patients. MRI was performed at least 1 month after AF ablation. The patients with an inadequate image quality of the RF lesion on DE-MRI were excluded from this study. The study was approved by the local institutional review board (date: 19.11.2013; approval number: 20), and written informed consent was obtained from all patients.

2.2. Mapping and ablation procedure

Prior to the procedure, transesophageal echocardiography was performed to exclude thrombus formation. The study was performed in spontaneously breathing patients under deep propofol sedation. Standard electrode catheters were placed in the right ventricular apex and the coronary sinus after which a single transseptal puncture was performed. Unfractionated heparin was administered in bolus form before the transseptal puncture to maintain an activated clotting time of >300 s. If AF was sustained, an internal electrical cardioversion was performed to restore sinus rhythm (SR). Mapping and ablation were performed using the CARTO3 system (Biosense Webstar, Diamond Bar, CA, USA) or the NavX system (St. Jude Medical, Inc., St. Paul, MI) as a guide after integration of a three-dimensional (3D) model of the LA and PV anatomy obtained from pre-interventional computed tomography (CT). Prior to the ablation, circular mapping catheter- (Lasso, Biosense Webster; Optima, St. Jude Medical Inc.) and ablation catheter-reconstructed posterior LA anatomies were aligned with the CT image. Fine adjustment of image integration was achieved through three additional landmarks (at the top of left superior PV, right superior PV, and at the bottom of left inferior PV); these landmarks were visited with the tip of the ablation catheter (Thermocool, Biosense Webster; IBI Therapy Cool Flex, St Jude Medical, Inc.) according to fluoroscopy and electrogram information. The RF alternating current was delivered in a unipolar mode between the irrigated tip electrode of the ablation catheter and an external back-plate electrode. The initial RF generator setting consisted of an upper catheter tip temperature of 43 °C, a maximal RF power of 30 W, and an irrigation flow rate of 13 ml/min. When RF application was performed on the posterior wall, the initial RF generator setting consisted of a maximal RF power of 20 W. All patients underwent PVI. RF application could be performed in a "point by point" fashion. The level of ablation was chosen on the atrial side of the PV antrum, mainly depending on the operator's decision. The maximum time at the anterior wall and posterior wall was 40 and 20 s, respectively. RF energy was routinely reduced by 10 W when ablating the posterior wall according to the esophageal temperature measured with an esophageal temperature probe (SensiTherm, St. Jude Medical Inc.). If the esophageal temperature rose to >39 °C, the ablation was immediately stopped and energy further reduced. After the esophageal temperature decreased to within the normal range (37 °C), RF application was resumed. If the ablation could not be performed with 20 W, the line placement was performed either more antral or closer to the PV, depending on the individual anatomical findings. Catheter navigation was performed with a non-steerable sheath (Preface, Multipurpose, Biosense Webster) or steerable sheath (Agilis, St. Jude Medical Inc.). The procedural end point was considered to be the electro-physiologically proven bidirectional block for the PV-encircling ablation lines confirmed with a circular mapping catheter. After confirming bidirectional block of the PV, we performed a stimulation protocol (burst pacing from coronary sinus (CS) with 300 ms, 250 ms, and 200 ms for 10 s each) for testing the inducibility. In those cases in which atrial fibrillation was induced, patients underwent cardioversion, and the procedure ended with patients in paroxysmal atrial fibrillation; a linear ablation including roof and mitral isthmus lines was added in the patients with persistent atrial fibrillation. A pharmacological test (high dose isoproterenol infusion: 20 μg/min) was performed in order to identify non-PV triggers. Ablation of the cavotricuspid isthmus was performed only if typical right atrial flutter was either documented previously or induced by burst pacing at the end of the procedure.

2.3. CE-MRA acquisition

CE-MRA of PV–LA anatomy was acquired with a breath-hold 3D T1 fast field echo (T1-FFE) sequence in the coronal plane during the first pass of a gadopentetate dimeglumine injection (Magnevist; Bayer Yakuhin, Osaka, Japan), at a dose of 0.1 mmol/kg of body weight. The acquisition time was approximately 15 s. This scan technique has been previously established, and the acquired image has been used for the AF ablation procedure [5–7].

2.4. DE-MRI acquisition

The scan technique and parameters for DE-MRI have been previously reported [8–11]. The DE-MRI of the LA with the PVs was acquired using a 3D inversion recovery, respiration navigated, electrocardiogram-gated, T1-FFE sequence in the transverse plane 15 min after the injection of 0.1 mmol/kg gadolinium as the contrast agent. The typical scan parameters were: repetition time (TR)/echo time (TE)=4.7/1.5, voxel size=$1.25 \times 1.26 \times 2.60$ mm^3 (reconstructed to $0.63 \times 0.63 \times 1.30$ mm^3), flip angle=15, inversion time (TI)=280–330 ms, SENSE with a reduction factor of 2, and 70 reference lines. The TI value was identified from the myocardial TI_{null} using a Look-Locker. The T1 of the LA wall was similar to the myocardial T1 [8]. The data acquisition was limited to 15% of the cardiac cycle. In cases of SR, during MRI, the data acquisition was performed during the mid-diastolic phase of the left ventricle. In case of AF, during MRI, the trigger delay of the cardiac synchronization was set to the shortest value. Saturation bands were placed in the phase-encoding (right–left) line to minimize back-folding from the arms. Fat saturation was used to suppress any fat signals. The typical scan time for the DE-MRI study was 7–12 min depending on the patient's heart rate and respiration pattern. An attempt to control the heart rate at <70 bpm was made using metoprolol 20 mg or 40 mg.

2.5. A 3D visualization of RF lesions

A 3D visualization and segmentation of the MRI were performed with AZE Virtual Place (AZE Virtual Place; AZE, Tokyo, Japan). The method for the 3D visualization has been reported previously [3,12,13]. Briefly, we segmented the LA wall and calculated the mean value and standard deviation (SD) of the pixel intensity histogram. The detailed method is as follows: (1) In CE-MRA data, a 3D image was segmented from the surrounding structures. The anatomical information obtained from the 3D CE-MRA indicated the endocardial border of the LA wall (end CE-MRA). (2) We prepared the modified CE-MRA data with 3 pixel enlarged volume automatically using the AZE software. The enlarged CE-MRA data indicated the epicardial border of the LA wall (epi CE-MRA). (3) In the DE-MRI data, the LA wall segmentation was performed automatically with the 2-segmented 3D-MRA

data (end and epi CE-MRA) using the fusion software. (4) The LA wall was segmented by subtracting from the epi CE-MRA to endo CE-MRA. Then, a voxel intensity histogram analysis of the LA wall identified the DEs as intensities >1 SD. Furthermore, the degree of intensity was categorized by color-coded scaling (green: 1 SD–2 SD: yellow: SD–3 SD; red: >4 SD) [14]. Finally, a 3D reconstruction of the LA and PV with the DEs was achieved automatically.

2.6. The 3D reconstruction of DE-MRI fused with CE-MRA

Source images of CE-MRA and DE-MRI were transferred to a workstation (AZE Virtual Place; AZE) and fused automatically. In the case of a suboptimal fusion image, the fusion was attempted manually by experienced radiological technicians. In regard to the fusion, the location of the LA in both must be same for achieving an excellent fusion of the CE-MRA and DE-MRI. Hence, we acquired the CE-MRA at the end-expiratory phase, as when acquiring the DE-MRI. The location of the LA changes dramatically in the expiratory and inspiratory phases. The algorithm for merging CE-MRA and DE-MRI is very simple and involves: (1) automatic adjustment of the 2 images using a positional reference as table location and (2) if the above is not optimal, manual adjustment is needed. The most important tips for successful fusion are as follows: (1) keeping patients awake during MRI acquisition and (2) reducing abdominal motion using a lumbago belt.

2.7. Comparison of the image quality: DE-MRI vs DE-MRI fused with CE-MRA

Two observers independently assessed the image quality of both DE-MRI and DE-MRI fused with CE-MRA. We divided the RF lesion around the pulmonary veins into the following 14 segments: anterior ridge segment of left superior PV (a-LSPV), anterior ridge segment of left inferior PV (a-LIPV), posterior segment of left inferior PV (p-LIPV), posterior segment of left superior PV (p-LSPV), roof segment of left superior PV (r-LSPV), bottom segment of left inferior PV (b-LIPV), carina segment of left PV (c-LPV), anterior segment of right superior PV (a-RSPV), anterior segment of right inferior PV (a-RIPV), posterior segment of right inferior PV (p-RIPV), posterior segment of right superior PV (p-RSPV), roof segment of right superior PV (r-RSPV), bottom segment of right inferior PV (b-RIPV), and carina segment of right PV (c-RPV) (Fig. 1). Image quality with regard to localization of RF lesion and adjacent LA and PV anatomy in each segment was assessed on AZE Virtual Place using a 3-point scale: 0=poor image quality, RF lesion and adjacent LA and PV anatomy only partly discernible; 1=good image quality, acceptable delineation of most parts of the RF lesion localization and adjacent LA–PV anatomy; 2=excellent image quality, clear delineation of the entire RF lesion localization and all adjacent LA–PV anatomy. A total image quality score (0–28) was calculated as a sum of scores in all segments.

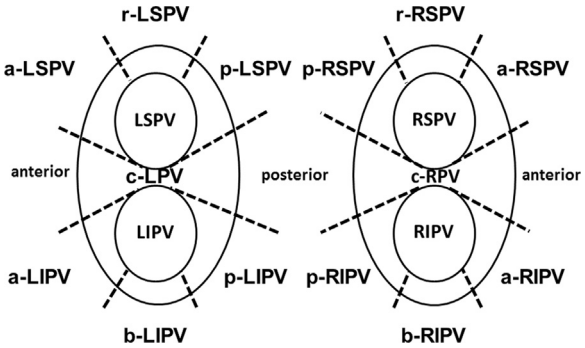

Fig. 1. The 14 segments for assessment of the image quality of both circular lesions. a-LSPV=anterior ridge segment of left superior PV, a-LIPV=anterior ridge segment of left inferior PV, p-LIPV=posterior segment of left inferior PV, p-LSPV=posterior segment of left superior PV, r-LSPV=roof segment of left superior PV, b-LIPV=bottom segment of left inferior PV, c-LPV=carina segment of left PV, a-RSPV=anterior segment of right superior PV, a-RIPV=anterior segment of right inferior PV, p-RIPV=posterior segment of right inferior PV, p-RSPV=posterior segment of right superior PV, r-RSPV=roof segment of right superior PV, b-RIPV=bottom segment of right inferior PV, and c-RPV=carina segment of right PV.

2.8. Inter- and intra-observer variability in the assessment of image quality

To assess inter-variability, 2 observers (2 experienced radiological technicians) scored the 3D reconstructed image on a scale of 0–2 in all 14 segments. The overall score (0–28) was defined as a sum of all segments. The observers then qualitatively assessed the relationship between observers 1 and 2. Furthermore, one of the 2 observers calculated all the cases again 1 month after the initial calculation to assess intra-observer variability. The observer was blinded to the results of the initial calculation.

2.9. Statistics

The data were tested using the Kolmogorov–Smirnov test and were presented as mean $\pm$ standard deviation for normally distributed variables. The median and quartiles are given for non-normally distributed variables. Continuous variables were analyzed using the Wilcoxon signed-rank test. Using a linear regression model, we evaluated inter- and intra-observer variability in scoring the image quality of both DE-MRI and DE-MRI fused with CE-MRA. A value of $p<0.05$ was considered statistically significant. All statistical analyses were performed with SPSS, Release 17.0 software (SPSS, Chicago, IL, USA).

3. Results

3.1. Patient characteristics

The patient characteristics are shown in Table 1. Most patients (12/18, 67%) had the paroxysmal type of AF. The median duration of AF history was 66 (37, 97) months. The left atrial diameter and left atrial appendage flow were 42 ± 6 mm and 50 ± 23 cm/s, respectively.

3.2. Cardiac rhythm, heart rate, and metoprolol use during MRI

The cardiac rhythm, heart rate, and metoprolol use during MRI are shown in Table 2. Most of the patients were in SR during the

Table 1
Clinical characteristics of the patients.

Age, years	60 ± 9
Male, *n* (%)	17 (88)
Type of AF, *n* (%)	
Paroxysmal	12 (67)
Persistent	6 (33)
AF history, months	66 (37, 97)
Antiarrhythmic drugs, *n*	0 (0, 1)
Arterial hypertension, *n* (%)	7 (39)
Diabetes mellitus, *n* (%)	4 (22)
Lone AF, *n* (%)	3 (17)
LAA flow (cm/s)	50 ± 23
Left atrial diameter (mm)	42 ± 6
LV ejection fraction (%)	57 ± 9

AF=atrial fibrillation, LV=left ventricle, and LAA=left atrial appendage.

MRI. The mean heart rate was 69 ± 11 bpm with metoprolol 20 mg or 40 mg.

3.3. A comparison of the image quality: DE-MRI vs DE-MRI fused with CE-MRA

A successful 3D reconstruction of the RF lesion and LA–PV anatomy was achieved by DE-MRI and CE-MRA in all patients, respectively. The images of both DE-MRI and DE-MRI fused with CE-MRA are shown in Fig. 2. The image quality score of each segment is shown in Table 3. The image quality score in all segments was likely to be higher in DE-MRI fused with CE-MRA than in DE-MRI. Of note, the image quality scores of the anterior ridge segment and carina segment of the left PV were significantly higher in DE-MRI fused with CE-MRA with both observers 1 and 2 (observer 1: r-LSPV: 1 (1, 2) vs 2 (2, 2), $p=0.001$, a-LSPV: 1 (0, 2) vs 2 (2, 2), $p=0.001$, a-LIPV: 1 (0, 2) vs 2 (2, 2), $p=0.004$, b-LIPV: 2 (1, 2) vs 2 (2, 2), $p=0.009$, c-LPV: 0 (0, 2) vs 2 (2, 2), $p=0.001$; observer 2: a-LSPV: 1 (1, 2) vs 2 (2, 2), $p=0.001$, a-LIPV: 1 (1, 2) vs 2 (2, 2), $p<0.001$, b-LIPV: 2 (1, 2) vs 2 (2, 2), $p=0.008$, c-LPV: 1 (0, 1) vs 2 (2, 2), $p<0.001$). The overall scores were significantly higher in the DEMRI fused with CE-MRA as compared with DE-MRI (observer 1: 22 (18, 25) vs 28 (28, 28), $p<0.001$; observer 2: 24 (23, 25) vs 28 (28, 28), $p<0.001$). Fig. 3 shows the representative case. The RF lesion gap at the anterior ridge could be completely visualized.

Table 2
Cardiac rhythm, heart rate, and metoprolol use during MRI.

Time to MRIafter AF ablation (days)	80 (49, 193)
Cardiac rhythm during MRI	
Sinus rhythm, *n* (%)	13 (73)
Atrial fibrillation, *n* (%)	5 (27)
Usage of metoprolol, *n* (%)	6 (33)
Dosage of metoprolol	
20 mg, *n* (%)	1 (6)
40 mg, *n* (%)	5 (28)
Heart rate (bpm)	69 ± 11

MRI = magnetic resonance image and AF = atrial fibrillation.

3.4. Inter- and intra-observer variability in the overall score

When estimating the image quality score, there was excellent correlation between observers 1 and 2, as well as the initial and the second calculation (inter-observer: $r=0.759$, $p<0.001$; intra-observer: $r=0.836$, $p<0.001$). This suggested that both inter- and intra-observer variability were within an acceptable range.

4. Discussion

4.1. Main findings

The RF lesion could be visualized by DE-MRI. Furthermore, the DE site was associated with the RF ablation area assessed by the electroanatomical mapping system. However, recognition of the DE site around the anterior ridge or carina region was difficult in

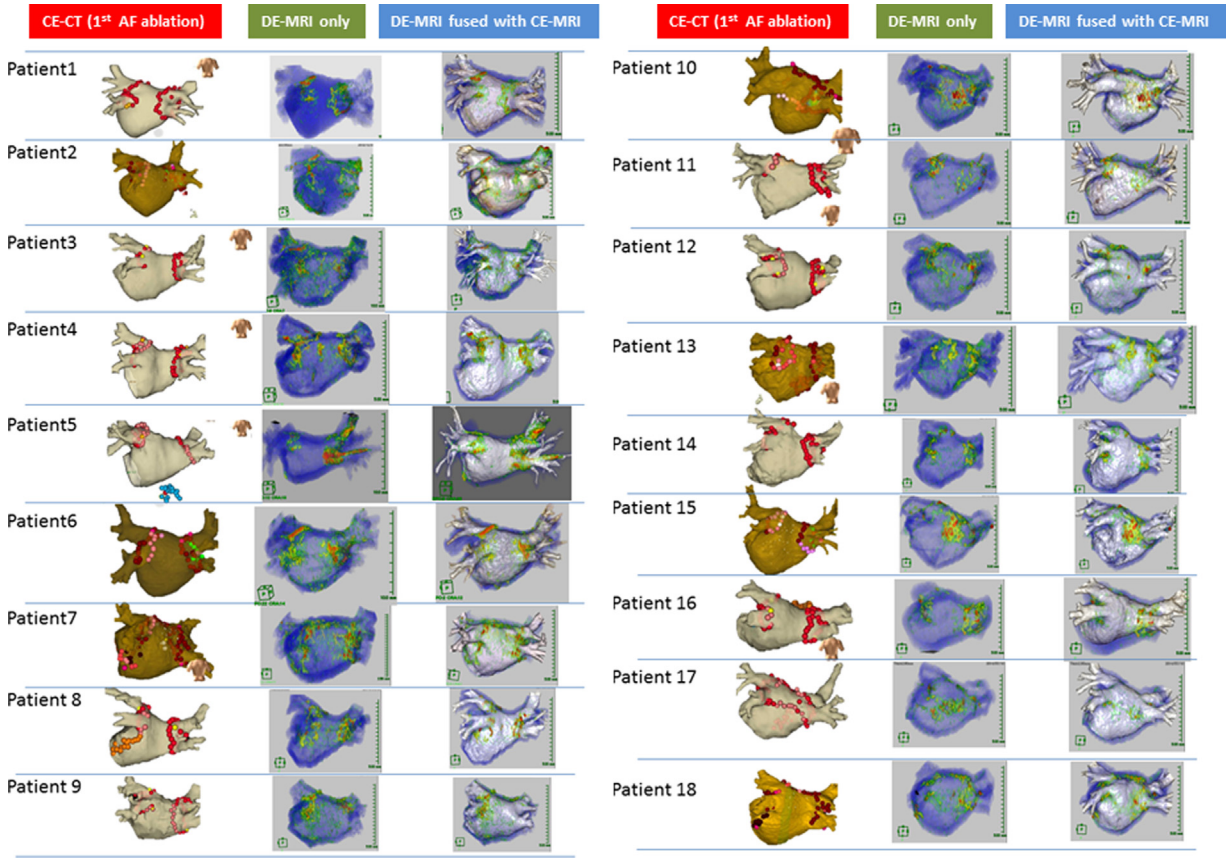

Fig. 2. Visualization of RF lesion using DE-MRI and DE-MRI fused with CE-MRA. Catheter ablation using NavX system or CARTO3 system integrated with 3D-CT in the 1st session. The 3D red tag indicates the ablation point. The 3D pink tag indicates the ablation point with a reduced power due to the esophageal temperature rise (left panel). Visualization of RF lesion using DE-MRI (middle panel). Visualization of RF lesion using DE-MRI fused with CE-MRA (right panel). RF = radio frequency; DE-MRI = delayed enhancement magnetic resonance imaging; CE-MRA = contrast-enhanced MRA.

Table 3
Image quality score by observer.

	Observer 1			Observer 2		
	DE-MRI ($n=18$)	DE-MRI fused with CE-MRA ($n=18$)	p-Value	DE-MRI ($n=18$)	DE-MRI fused with CE-MRA ($n=18$)	p-Value
Image quality score of each segment						
r-LSPV	1 (1, 2)	2 (2, 2)	0.001	2 (2, 2)	2 (2, 2)	1.00
a-LSPV	1 (0, 1)	2 (2, 2)	0.001	1 (1, 2)	2 (2, 2)	0.001
a-LIPV	1 (0, 2)	2 (2, 2)	0.004	1 (1, 2)	2 (2, 2)	<0.001
b-LIPV	2 (1, 2)	2 (2, 2)	0.009	2 (1, 2)	2 (2, 2)	0.008
p-LIPV	2 (2, 2)	2 (2, 2)	1.00	2 (2, 2)	2 (2, 2)	1.00
p-LSPV	2 (2, 2)	2 (2, 2)	0.32	2 (2, 2)	2 (2, 2)	0.32
c-LPV	0 (0, 2)	2 (2, 2)	0.001	1 (0, 1)	2 (2, 2)	<0.001
r-RSPV	2 (2, 2)	2 (2, 2)	0.04	2 (2, 2)	2 (2, 2)	1.00
a-RSPV	2 (2, 2)	2 (2, 2)	0.10	2 (2, 2)	2 (2, 2)	0.32
a-RIPV	2 (2, 2)	2 (2, 2)	0.06	2 (2, 2)	2 (2, 2)	0.16
b-RIPV	2 (1, 2)	2 (2, 2)	0.04	2 (2, 2)	2 (2, 2)	1.00
p-RIPV	2 (2, 2)	2 (2, 2)	0.32	2 (2, 2)	2 (2, 2)	1.00
p-RSPV	2 (2, 2)	2 (2, 2)	0.18	2 (2, 2)	2 (2, 2)	0.32
c-RPV	2 (2, 2)	2 (2, 2)	0.06	2 (1, 2)	2 (2, 2)	0.007
Overall image quality score						
	22 (18; 25)	28 (28; 28)	<0.001	24 (23; 25)	28 (28; 28)	<0.001

LSPV=left superior pulmonary vein, LIPV=left inferior pulmonary vein, RSPV=right superior pulmonary vein, RIVP=right inferior pulmonary vein, r=roof, a=anterior, b=bottom, p=posterior, c=carina, DE-MRI=delayed enhancement magnetic resonance imaging, and CE-MRA=contrast-enhanced angiography.

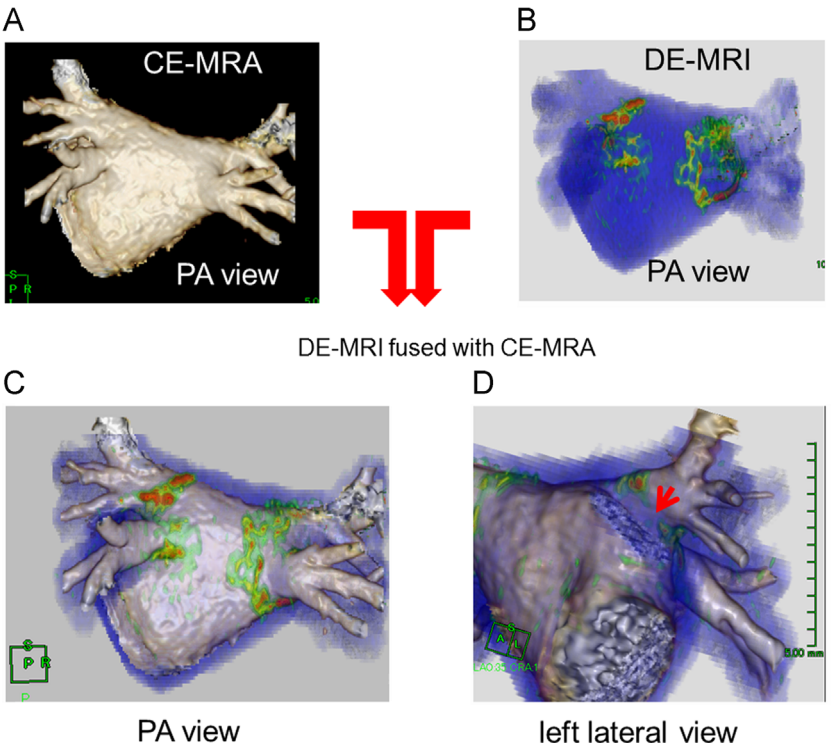

Fig. 3. Image quality of the DE-MRI fused with CE-MRA. (A) The 3D reconstructed image using CE-MRA, (B) the 3D reconstructed image using DE-MRI, and (C, D) the 3D reconstructed image using DE-MRI fused with CE-MRA. Of note, the RF lesion gap at the anterior ridge could be recognized (D). CE-MRA=contrast enhanced magnetic resonance angiography; DE-MRI=delayed enhancement magnetic resonance imaging; PA=postero-anterior.

some cases due to the complex anatomy and technical limitations of DE-MRI. The study presented here demonstrated that DE-MRI fused with CE-MRA could compensate for the disadvantages associated with the use of DE-MRI.

4.2. Insufficient anatomical information of DE-MRI: What is necessary for finding the RF lesion gap?

As estimating the quality of RF lesion, it is critical where the RF lesion gap was located.

The RF lesion gap was located at anterior segment of the left PV and posterior of right PV in most cases due to the inadequate energy delivery or inadequate contact force as well as the complex anatomy [15,16]. Thus, precise anatomical information about this area is essential for assessing the RF lesion gap around the PV. We have previously reported the visualization of RF lesion using DE-MRI. In our experience, the RF lesion around the posterior wall could be visualized completely. In contrast, the RF lesion around the anterior ridge and carina region was not visible in some cases. DE-MRI could not provide the precise anatomy including that of

the anterior ridge and carina region due to technical limitations and the complex anatomy of the PV and LA. To find the RF lesion gap, precise anatomical information, especially of the anterior ridge and carina region, is necessary. This may be the main reason for catheter ablation of AF using DE-MRI not being developed despite several studies reporting detection of RF lesion using DE-MRI; AF fibrosis has also been reported [17–19].

4.3. Limitation of the specialized software for visualizing the DE site

Several algorithms for segmentation of RF lesion or atrial fibrosis form DE-MRI have been reported. We recognized that currently no algorithm is deemed clearly better than others [20]. Visualization of the RF lesion or atrial fibrosis needs specialized software for the specific algorithm. The specialized software could provide complete visualization of the DE site, but not the precise anatomy around the anterior ridge and carina region. We considered that DE-MRI using the current algorithm could not improve the anatomical resolution. Thus, we developed the fusion method, in which DE-MRI was fused with CE-MRA. The main advantage of this method is the visualization of DE at the anterior ridge and carina region of the left PV.

4.4. Clinical applicability of DE-MRI fused with CE-MRA

In the current study, the fusion of DE-MRI and CE-MRA as well as the visualization of RF lesion were completed with commercially available software. Recently, Bisbal et al. reported the MRI-guided approach to localize and ablate gaps in a repeat AF ablation procedure. In their study, all DE-MRI images were analyzed with self-customized software. A 3D shell was obtained from the DE-MRI. The resulting processed image of the selected shell was used to create a DE-MRI model that was integrated in the 3D electro-anatomical mapping system [21]. The image quality of the DE site was clear around the posterior wall and right PV. However, the quality of the images of the DE site around the left PV, especially the anterior ridge or carina region of left PV, was still not clear. Of note, the image quality of the shell, which was integrated with a 3D mapping system, was limited by the image quality acquired from DE-MRI. Thus, we believe that the resolution of this issue is the use of the high resolution image quality acquired by CE-MRA. With regard to the complexity and time required for acquiring both DE-MRI and CE-MRA, the technique is likely well established. Acquisition of CE-MRA was performed immediately after the gadolinium injection and before the acquisition of DE-MRI. We believe that the safety of this technique could be established for the patients.

4.5. Study limitations

Our study has 5 major limitations. First, the sample size was small. Second, the relationship between the gap assessed by DE-MRI and PV–LA re-conduction could not be demonstrated because a second AF procedure was not performed. This relationship should be investigated in a future study. Third, most of the patients were in SR during MRI acquisition. We could not endorse the image quality of MRI in patients with AF during MRI acquisition. Fourth, we may have overestimated the size of the RF lesion, because we had not previously assessed the original atrial fibrosis using DE-MRI before AF catheter ablation in most of the patients. Finally, our fusion method could not improve the image quality of RF lesion visualization on DE-MRI. Thus, an adequate image quality should be acquired by DE-MRI.

5. Conclusion

Visualization of RF lesion after pulmonary vein isolation can be accomplished with DE-MRI fused with MRA, which provides more precise anatomical information of the RF lesion compared to DE-MRI.

Disclosures

None.

Conflicts of interest

None.

Acknowledgments

None.

References

[1] Kiuchi K, Kircher S, Watanabe N, et al. Quantitative analysis of isolation area and rhythm outcome in patients with paroxysmal atrial fibrillation after circumferential pulmonary vein antrum isolation using the pace-and-ablate technique. Circ Arrhythm Electrophysiol 2012;5:667–75.
[2] Haissaguerre M, Jais P, Shah DC, et al. Spontaneous initiation of atrial fibrillation by ectopic beats originating in the pulmonary veins. N Engl J Med 1998;339:659–66.
[3] Kiuchi K, Okajima K, Shimane A, et al. Visualizing radiofrequency lesions using delayed – enhancement magnetic resonance imaging in patients with atrial fibrillation: a modification of the method used by the University of Utah group. J Arrhythm 2014. http://dx.doi.org/10.1016/j.joa.2014.06.005 (in press).
[4] Fahlenkamp UL, Lembcke A, Roesler R, et al. ECG-gated imaging of the left atrium and pulmonary veins: intra-individual comparison of CTA and MRA. Clin Radiol 2013;68:1059–64.
[5] Scaglione M, Biasco L, Caponi D, et al. Visualization of multiple catheters with electroanatomical mapping reduces X-ray exposure during atrial fibrillation ablation. Europace 2011;13:955–62.
[6] Dong J, Dickfeld T, Dalal D, et al. Initial experience in the use of integrated electroanatomic mapping with three-dimensional MR/CT images to guide catheter ablation of atrial fibrillation. J Cardiovasc Electrophysiol 2006;17:459–66.
[7] Noseworthy PA, Malchano ZJ, Ahmed J, et al. The impact of respiration on left atrial and pulmonary venous anatomy: implications for image-guided intervention. Heart Rhythm: Off J Heart Rhythm Soc 2005;2:1173–8.
[8] Peters DC, Wylie JV, Hauser TH, et al. Detection of pulmonary vein and left atrial scar after catheter ablation with three-dimensional navigator-gated delayed enhancement MR imaging: initial experience. Radiology 2007;243:690–5.
[9] Daccarett M, Badger TJ, Akoum N, et al. Association of left atrial fibrosis detected by delayed-enhancement magnetic resonance imaging and the risk of stroke in patients with atrial fibrillation. J Am Coll Cardiol 2011;57:831–8.
[10] Kuppahally SS, Akoum N, Badger TJ, et al. Echocardiographic left atrial reverse remodeling after catheter ablation of atrial fibrillation is predicted by preablation delayed enhancement of left atrium by magnetic resonance imaging. Am Heart J 2010;160:877–84.
[11] Akoum N, Fernandez G, Wilson B, et al. Association of atrial fibrosis quantified using LGE-MRI with atrial appendage thrombus and spontaneous contrast on transesophageal echocardiography in patients with atrial fibrillation. J Cardiovasc Electrophysiol 2013;24:1104–9.
[12] Kiuchi K, Okajima K, Shimane A, et al. Delayed-enhancement magnetic resonance imaging could detect the substrate of an unusual macroreentrant atrial tachycardia? J Cardiovasc Electrophysiol 2014;25:1032–3.
[13] Kiuchi K, Okajima K, Shimane A, et al. Visualization of pulmonary vein–left atrium reconduction site on delayed-enhancement magnetic resonance imaging in the second atrial fibrillation catheter ablation. Circ J 2014;78:2993–5.
[14] Oakes RS, Badger TJ, Kholmovski EG, et al. Detection and quantification of left atrial structural remodeling with delayed-enhancement magnetic resonance imaging in patients with atrial fibrillation. Circulation 2009;119:1758–67.
[15] Neuzil P, Reddy VY, Kautzner J, et al. Electrical reconnection after pulmonary vein isolation is contingent on contact force during initial treatment: results from the EFFICAS I study. Circ Arrhythm Electrophysiol 2013;6:327–33.
[16] Kimura M, Sasaki S, Owada S, et al. Comparison of lesion formation between contact force-guided and non-guided circumferential pulmonary vein isolation: a prospective, randomized study. Heart Rhythm 2014;11:984–91.

[17] Parmar BR, Jarrett TR, Burgon NS, et al. Comparison of left atrial area marked ablated in electroanatomical maps with scar in MRI. J Cardiovasc Electrophysiol 2014;25:457–63.
[18] McGann C, Akoum N, Patel A, et al. Atrial fibrillation ablation outcome is predicted by left atrial remodeling on MRI. Circ Arrhythm Electrophysiol 2014;7:23–30.
[19] Marrouche NF, Wilber D, Hindricks G, et al. Association of atrial tissue fibrosis identified by delayed enhancement MRI and atrial fibrillation catheter ablation: the DECAAF study. J Am Med Assoc 2014;311:498–506.
[20] Karim R, Housden RJ, Balasubramaniam M, et al. Evaluation of current algorithms for segmentation of scar tissue from late gadolinium enhancement cardiovascular magnetic resonance of the left atrium: an open-access grand challenge. J Cardiovasc Magn Reson 2013;15:105.
[21] Bisbal F, Guiu E, Cabanas-Grandio P, et al. MRI-guided approach to localize and ablate gaps in repeat AF ablation procedure. JACC Cardiovasc Imaging 2014;7:653–63.